A pair-potentials analysis of the emission spectroscopy of $^3P_1$ state atomic mercury isolated in solid Ar, Kr, and Xe

Cite as: J. Chem. Phys. **119**, 11888 (2003); https://doi.org/10.1063/1.1623174
Submitted: 23 April 2003 . Accepted: 10 September 2003 . Published Online: 21 November 2003

Martin A. Collier, and John G. McCaffrey

A pair-potentials analysis of the emission spectroscopy of $^3P_1$ state atomic mercury isolated in solid Ar, Kr, and Xe

Martin A. Collier and John G. McCaffrey
Department of Chemistry, National University of Ireland, Maynooth, Co. Kildare, Ireland

(Received 23 April 2003; accepted 10 September 2003)

Pair-potentials calculations of the $^3P_1 \leftrightarrow {}^1S_0$ absorption and emission energies of atomic mercury isolated in solid Ar, Kr, and Xe are conducted and compared with the spectral bands recorded in Hg/RG matrices. The Hg·RG pair potentials used are derived from spectroscopic studies of the mercury atom–rare gas atom diatomics and are implemented in a localized $Hg \cdot RG_{18}$ cluster model to simulate the spectroscopy of Hg atoms isolated in substitutional sites of the solid rare gases. The calculated absorptions are all on the red wing of the observed matrix bands and from these favorable comparisons, substitutional site occupancy is identified for ground state atomic mercury. A pairwise sum of the $Hg(^3P_1) \cdot RG$ $[A\,{}^3 0^+ (^3\Pi)]$ and $[B\,{}^3 1]$ state potentials is used to examine the vibronic modes of the excited $^3P_1$ state $Hg \cdot RG_{18}$ clusters which lead to stabilization. The energetics of waist and body vibronic modes, involving motion of the lattice atoms with respect to the excited state mercury atom and motion of this atom in the solid, respectively, were calculated for the three symmetry poles of the cubo-octahedral substitutional sites. Excited state stabilization was found for the waist mode of all the Hg/RG systems in the three possible coordinate systems, i.e., based on the fourfold, threefold, and twofold symmetry systems. In contrast, the body modes were stabilized only in Hg/Xe. The difference between Hg/Xe and the other Hg/RG systems is related to the larger substitutional site size presented by the former system. The three components identified in the recorded emission bands are correlated with the existence of several vibronic modes leading to stabilization. Emission energies calculated for the three stabilized vibronic modes in Ar are centered on the observed emission but exhibit a larger splitting. In Kr they are red of the observed band maximum but occur within the observed band. A curve crossing mechanism is identified which can explain the lack of emission for the strongly stabilized, fourfold symmetry modes in Hg/Xe.
 [DOI: 10.1063/1.1623174]

I. INTRODUCTION

The most detailed spectroscopic study of matrix-isolated[1] atomic mercury (Hg/RG) has focused on the $6p\,{}^3P_1 \leftrightarrow 6s\,{}^1S_0$ transition and was conducted a decade ago by the Orsay group.[2] Very recently our Group at Maynooth has extended[3] the experimental work because of the need to examine aspects of the Hg/RG matrix emission revealed in Hg·RG pair-potentials[4] simulations. The new experimental work has shown that the $^3P_1$ emission bands are multicomponent, requiring the use of three broad Gaussian functions to obtain satisfactory fits. Excitation spectra recorded for these emission components were all identical, indicating that the effect arises from single site occupancy. In this paper we present details of the pair-potential calculations and highlight aspects of the luminescence that were not evident in the original experimental work, in particular the quenching of very strongly bound excited states in the Hg/Xe system.

A localized, pair-potentials approach[5] is used to investigate the characteristics of the absorption and emission spectroscopy of atomic mercury isolated in rare gas solids. The validity of the pair potentials approach has been examined by Beswick *et al.*[6] for the triatomic $Hg(^3P_1) \cdot Ar_2$ complex by simulating the vibronic structure in the resonance two-photonionization (R2PI) spectra recorded for this cluster by Jouvet and co-workers.[7] A similar theoretical approach has also been used by Alexander and co-workers[8] on the ground state $B(^2P_J) \cdot Ar_2$ system. McCaffrey and Kerins[5] adapted Beswick's cluster method for the solid state in a simulation of the spectroscopy of atomic zinc in the solid rare gases. The calculations originally employed for zinc were recently extended to cover atomic cadmium[9] and in the present paper, the method is developed further for atomic mercury.

In the following sections, an examination of the Hg atom $^3P_1 \leftrightarrow {}^1S_0$ matrix spectroscopy is presented using experimental Hg·RG pair potentials for the ground X and excited A and B states[6,10,11] in $Hg \cdot RG_{18}$ cluster calculations. In addition to the tetragonal (fourfold symmetry) ''body'' (Q_2) and ''waist'' (Q_3) modes described in our earlier work,[5,9] calculations of trigonal (threefold symmetry) six-atom ''body'' (Q_4) and ''waist'' (Q_5), modes are performed on the Hg/RG systems. Details of the twofold symmetry body (Q_6), and waist (Q_7), modes are also presented for each of the excited state p-orbital orientations. The new calculations presented in this contribution cover the three symmetry poles of a cubo-octahedral point group[12] to which the $M \cdot RG_{12}$ system belongs. This high symmetry approach has been adopted as it provides the most extreme energetics, i.e., the attractive orbital orientations yield the most stabilized energies while the repulsive orientations are the most destabilized. All lower symmetry selections will provide intermediate energies be-

tween these extreme values. In the high symmetry approach insight can be gained especially into the stabilized modes which determine the excited state relaxation and produce emission. This insight is lost in methods, such as Monte Carlo or molecular dynamics calculations where the Z axis is not space fixed.

For the purpose of illustration, a full account of the interaction details is presented for Hg/Xe while only a summary, showing stabilized modes is provided for the Hg/Ar and Hg/Kr systems. Predictions made in the theoretical analysis are compared with matrix absorption and emission spectra recorded by our group at Maynooth, revealing information on the site occupancy and excited state dynamics.

II. METHODS AND RESULTS

The methods used to determine the ground and excited state energies of $(ns)^2$ metal atoms occupying substitutional sites in Ar, Kr, and Xe lattices have been outlined in our earlier work on the Zn/RG[5] and Cd/RG[9] matrix systems. The calculations undertaken probe large amplitude vibrational motions which in the high symmetries selected, produce distinct electronic states. These calculations do not adequately probe the region of degeneracy in the excited electronic state which would involve small amplitude vibrational displacements around the ground state equilibrium configurations. Thus the latter calculations will give a better description of absorption while our calculations best describe the emission spectroscopy.

Briefly, the energy of a guest metal atom (M) occupying a substitutional site in a solid rare gas (M/RG) system is calculated for an $M \cdot RG_{18}$ cluster. The rare gas atoms in this cluster fall, as shown in Fig. 1, into two categories based on whether they are located in the first or second sphere of host atoms surrounding the guest atom M. The first category has a cubo-octahedral arrangement of 12 host atoms located at a nearest neighbor (NN) distance of $a/\sqrt{2}$ from M. The other set, consisting of six atoms are located at a next nearest neighbor (NNN) distance of the lattice parameter, a, from the guest atom and are arranged as a regular octahedron on the X, Y, and Z axes.

A. Ground $^1S_0$ state

The most fundamental aspect of the solid state calculations is the site occupied by the ground state metal atom in the rare gas lattices. From the ground state bond length (R_e) data presented in Table I for the mercury atom–rare gas atom diatomics and the rare gas dimers, very good matches exist between the Xe_2 and Kr_2 systems and their $Hg \cdot RG$ counterparts. Very favorable matches also exist for the $Hg \cdot RG$ van der Waals bond lengths and the substitutional site (SS) sizes of the solid rare gases. Thus in solid Xe, SS is 4.334 Å, calculated from the lattice parameter[13] $a = 6.13$ Å, while the $Hg \cdot Xe$ bond length is 4.25 Å and in solid Kr, SS is 3.991 Å while R_e $Hg \cdot Kr$ is 4.07 Å. The match that exists for Hg in Ar is not quite as good, where SS is 3.756 Å and R_e $Hg \cdot Ar$ is 3.98 Å. However, even in Hg/Ar, substitutional site occupancy is also expected.[14]

Comparison of the predicted and observed absorption

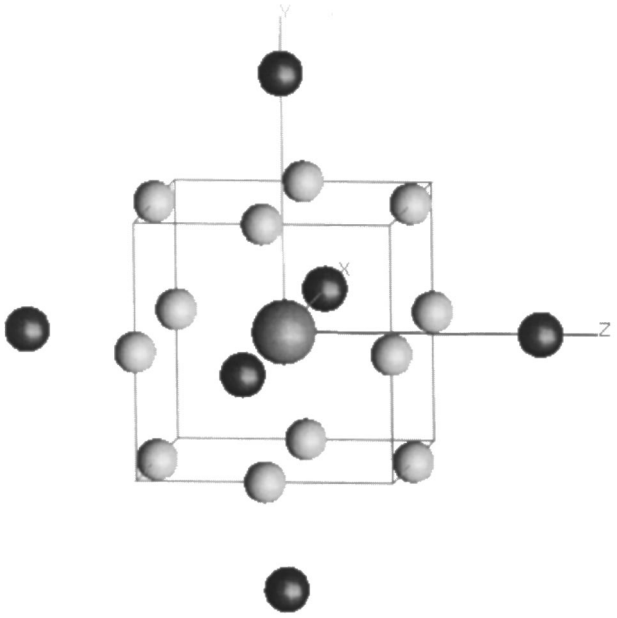

FIG. 1. The guest atom-based coordinate system used to calculate the energy of a metal atom, M in a substitutional site of an fcc lattice. The 12 nearest neighbor (NN) Rg atoms surrounding the guest atom located at the origin are shown as gray spheres on the edges of the cubic unit cell. The six next nearest neighbor (NNN) atoms in the second surrounding sphere are shown as the dark spheres on the X, Y, Z axes at the lattice parameter distance, a, from the guest metal atom. The axis system shown is coincident with the three, fourfold (C_4) symmetry axes of the cubo-octahedral fcc unit cell and is referred to in the text as four-atom mode calculations. The image was generated by the gOpenMol (Ref. 21) program.

energies[2] is used to examine if substitutional sites are occupied by atomic mercury. This is achieved with the expression

$$W_X(R) = \sum_{k=1}^{n} V^X_{\mathrm{Hg-Rg}}(R_k) + \sum_{i=1}^{m} V^X_{\mathrm{Rg-Rg}}(r_i) \qquad (1)$$

which gives the ground state energy of the cluster as a sum of the $Hg \cdot RG$ and RG_2 pair potentials. The simple summation of the pair potentials in Eq. (1) is possible due to the spherical symmetry of the ground $6s^2\,{}^1S_0$ state mercury atom. Morse functions are used for the ground state potentials for the $Hg \cdot RG$ diatomics and the rare gas dimers, RG_2 (Rg=Ar, Kr, and Xe). The parameters used for these functions are listed in Table I.

B. Excited $^3P_1$ state

In order to calculate the mercury atom $6p\,{}^3P_1 \leftrightarrow 6s\,{}^1S_0$ absorption and emission energies in the solid, it is necessary to obtain the energy of the electronically excited $^3P_1$ state metal atom in the $M \cdot RG_{18}$ cluster. To achieve this, the general cluster expression[6] for a $J=1$ electronic level is utilized. The three $6p$ orbitals of the excited $^3P_1$ state mercury atom give rise to the following cluster states:

$$(p_z) \quad W_1(R) = \sum_{k=1}^{n} \cos^2\theta_k V_\Sigma(R_k) + \sin^2\theta_k V_\Pi(R_k), \quad (2)$$

TABLE I. Spectroscopic constants used to generate the Morse potential energy curves for the Hg·RG and RG_2 diatomics. Data source are indicated by the references.

Hg·RG state	Morse parameters	Hg·Ar (Ref. 6)	Hg·Kr (Refs. 10 and 11)	Hg·Xe (Ref. 10)
$X\,^1\Sigma$	μ_{Hg-RG} (amu)	33.361 4162	59.281 9820	79.792 6882
($^10^+$)	$D_e(cm^{-1})$	130.25	178	254
	$\omega_e(cm^{-1})$	23.5	20	18.3
	$\omega_e x_e(cm^{-1})$	1.1	0.54	0.33
	R_e(Å)	3.98	4.07	4.25
	$\beta(Å^{-1})$	1.448 348	1.405 57	1.249 072
$A\,^3\Pi$	$D_e(cm^{-1})$	353.63	517 (628.7)	1380.9
($^30^+$)	$\omega_e(cm^{-1})$	41.2	43.5 (40.63)	54.17
	$\omega_e x_e(cm^{-1})$	1.2	1.5 (0.691)	0.565
	R_e(Å)	3.34	3.52 (3.35)	3.15
	$\beta(Å^{-1})$	1.541 049 64	1.793 813 (1.519 3512)	1.585 736
$B\,^3\Sigma$	$D_e(cm^{-1})$	51.57	96 (104.8)	187.6
(^{31})	$\omega_e(cm^{-1})$	11.4	11.3 (11.1)	9.71
	$\omega_e x_e(cm^{-1})$	0.6	0.32 (0.301)	0.215
	R_e(Å)	4.66	4.57 (4.58)	4.47
	$\beta(Å^{-1})$	1.116 6067	1.081 374 (1.016 6592)	0.771 18
		Ar·Ar (Ref. 20)	Kr·Kr (Ref. 20)	Xe·Xe (Ref. 20)
$X\,^1\Sigma$	$D_e(cm^{-1})$	99.545	138.4	196.24
	R_e(Å)[a]	3.7565	4.017	4.3634
	$\beta(Å^{-1})$	1.402 18	1.604	1.509

[a]Small differences which exist between the substitutional site sizes (calculated from the crystal lattice parameters) of rare gas atoms in the solid state and the equilibrium ground state bond lengths of the rare gas dimers in the gas phase arise from weak multibody effects occurring in the solid state.

$$(p_x)W_2(R)=\sum_{k=1}^{n}\sin^2\theta_k\cos^2\phi_k V_\Sigma(R_k)+[\cos^2\theta_k\cos^2\phi_k+\sin^2\phi_k]V_\Pi(R_k), \quad (3)$$

$$(p_y)W_3(R)=\sum_{k=1}^{n}\sin^2\theta_k\sin^2\phi_k V_\Sigma(R_k)+[\cos^2\theta_k\sin^2\phi_k+\cos^2\phi_k]V_\Pi(R_k), \quad (4)$$

where n is number of metal–rare gas bonds in the cluster. In contrast to the ground state potential [Eq. (1)], the excited state energy is no longer a simple sum of the $V_\Pi(R)$ and $V_\Sigma(R)$ pair potentials, but depends on the angle variables[5] θ_k and ϕ_k. In a Cartesian coordinate system having the metal atom positioned at the origin, θ_k is the angle subtended between a rare gas atom k and the Z axis, while ϕ_k is the angle obtained by projecting the vector connecting this atom and the origin onto the XY plane.

The $V_\Pi(R)$ and $V_\Sigma(R)$ terms appearing in Eqs. (2)–(4) are the pure Π and pure Σ spatial state potentials and not the spectroscopic A and B states of the Hg·RG diatomics presented in Table I. As the $B(\Omega_A=\pm1)$ state is a linear combination of Π and Σ orientations, it is necessary to extract the pure Σ potential for use in Eqs. (2)–(4). This was achieved using the relationship[15] $V_B=\frac{1}{2}[V_\Sigma^e+V_\Pi^e]$ which yields

$$V_\Sigma(R)=2V_B(R)-V_A(R), \quad (5)$$

the spatial Σ component of the original B state. Since the $A(\Omega_A=0)$ state is of pure Π symmetry[15] ($V_A=V_\Pi^e$) this potential was used directly. The result of the deconvolution of the pure Σ component from the B state is shown in Fig. 2 for the Hg·RG diatomics (RG=Ar, Kr, and Xe).

It is clear in Fig. 2 (dashed line) that the Σ states deconvoluted with Eq. (5) are not completely repulsive as they all show weakly bound regions at long range. This behavior is consistent with a very slightly attractive van der Waals interaction which exists between the metal atom M(p_z) orbital and the rare gas atoms. At very short range, however, it was observed for all the Hg·RG systems, that the deconvoluted Σ state curves exhibited a nonphysical minimum, instead of increasing exponentially like the B state. Fortunately, this nonphysical behavior of the Σ state (not shown in the plot) does not occur in the range of distances involved in the solid state simulations. Even in Hg·Xe, the worst case of the Hg·RG diatomics, the Σ state becomes nonphysical at distances less than 2.8 Å. As this is less than the shortest distance encountered for substitutional site occupancy (3.065 Å, half the lattice parameter of Xe), the raw deconvoluted Σ potential was used in all the excited state calculations.

Excited $^3P_1$ state energies were calculated for the body and waist vibronic (2) modes for the three p-orbital (3) orientations. The energetics of the two modes and the three orbital orientations were determined for three coordinate systems based on the three symmetry poles (3) of the cuboctahedron. The symmetry poles[12] are fourfold, threefold, and twofold symmetric and their calculations are referred to in this presentation as four-atom, six-atom, and two-atom modes, respectively. Thus for a given rare gas host, a total of 18 excited state potential energy curves were calculated for an Hg·RG_{18} cluster. Energies of the coordinate displace-

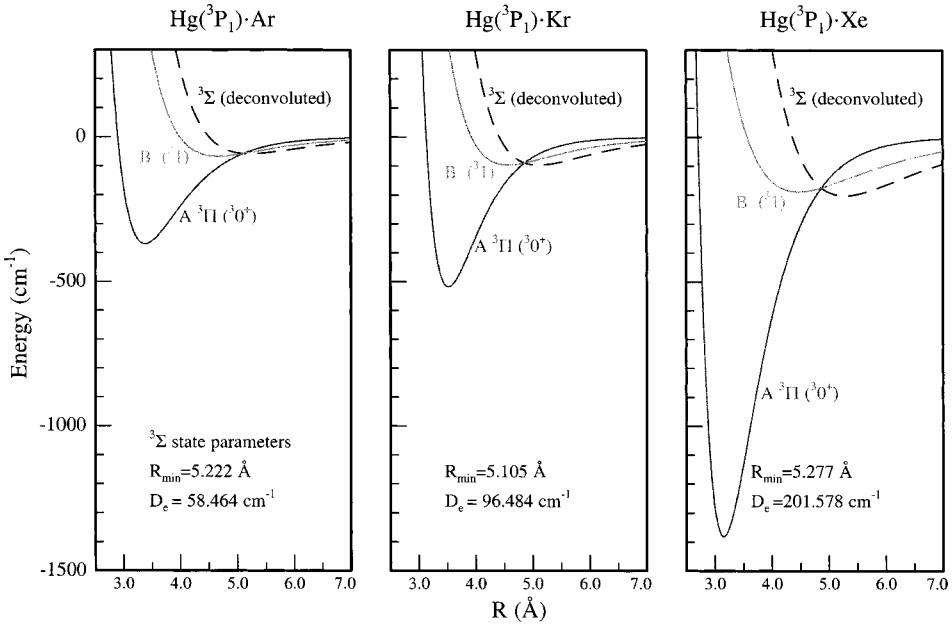

FIG. 2. The $Hg(^3P_1)\cdot RG\,^3\Sigma$ states extracted with Eq. (5) from the spectroscopic $[A\,^30^+(^3\Pi)]$ and $[B\,^31]$ states whose constants are given in Table I. All of these states share the Hg atom $6p\,^3P_1$ asymptote at 39 424.1 cm^{-1} but are shown dissociating to zero energy for the purpose of comparison. Note that all the deconvoluted $Hg\cdot RG\,^3\Sigma$ states show a weakly bound region at long internuclear distance. These distances are listed as R_{min} in the plots while the binding energies are indicated by D_e.

ments were calculated at 0.001 Å intervals. As a check of the correctness of our code, absorption energies were compared for the three coordinate systems calculated. This can be used as a check since the three p orbitals are degenerate at the center of the cubo-octahedral substitutional site. Hence at $R=0$, all modes must produce identical absorption values irrespective of the vibronic mode, the symmetry coordinate system used or the orbital.

1. Tetragonal (four-atom) symmetry modes

By choosing, as shown in Fig. 1, the Cartesian coordinate system to coincide with the three fourfold symmetry axes of the cubo-octahedron, the general sum expressions given by Eqs. (2)–(4), reduce[5] to the simpler product expressions

$$W_{3A1}(R)=4[\cos^2\theta V_{3\Sigma}(R)+\sin^2\theta V_{3\Pi}(R)], \quad (6)$$

$$W_{3E}(R)=2[\sin^2\theta V_{3\Sigma}(R)+(\cos^2\theta+1)V_{3\Pi}(R)] \quad (7)$$

which give the energies of the $^3A(p_z)$ and doubly degenerate $^3E(p_x,p_y)$ states of an excited $^3P_1$ state metal atom in a substitutional site. Equation (7) was obtained upon summation of the expressions resulting after substituting values of $\phi_k=k\pi/4$, $k=1$, 2, 3, and 4 in Eqs. (3) and (4).

a. The body mode: (Q_2) is the four-atom body mode presented in our earlier work[5] on the Zn/RG systems. It involves motion of the excited state metal atom along the Z axis from the center of the substitutional site towards the octahedral interstitial site located on the face of the unit cell. In the present contribution, the energetics of the Q_2 mode are presented not only for the p_z orientation but also for the degenerate p_x/p_y set. These orientations correspond to the ^3A and ^3E states, respectively, of the excited Hg atom in a substitutional site. They are shown for Hg/Xe in the upper half of Fig. 3. Clearly the p_z orbital orientation is the only one exhibiting stabilization for the four-atom body mode, Q_2. As the legend in Fig. 3 reveals ($I_{oh}1$, dashed line), stabilization is due to the approach of $Hg(p_z)$ to the octahedral interstitial site.

b. The waist mode: (Q_3) involves contraction of four host atoms on a non-close-packed plane towards the central metal atom. The overall energy of this vibronic mode of the $M\cdot RG_{18}$ cluster is obtained[5] as a sum of the four fourfold symmetry moieties making up what are the first and second spheres surrounding the metal atom in a substitutional site and the lattice contribution. Results calculated for the Q_3

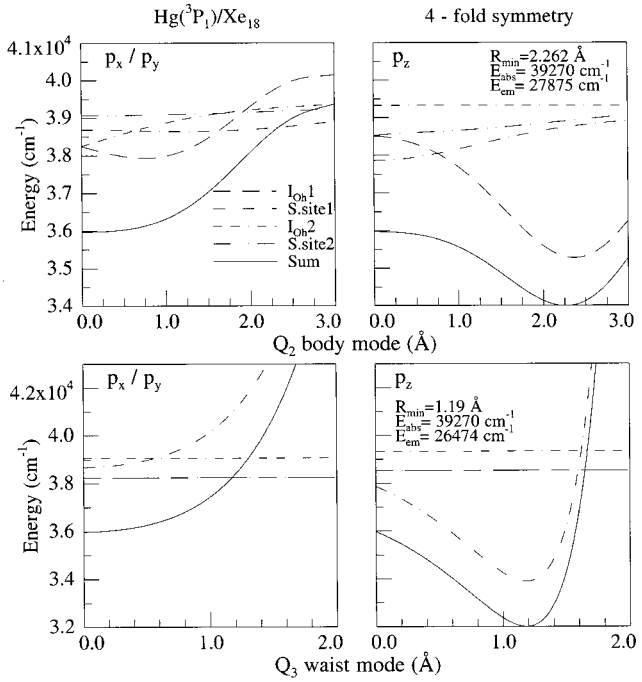

FIG. 3. Potential energy curves calculated for the four-atom (tetragonal, Q_2 and Q_3) modes based on substitutional site (SS) occupancy of the Hg atom in the Hg/Xe system.

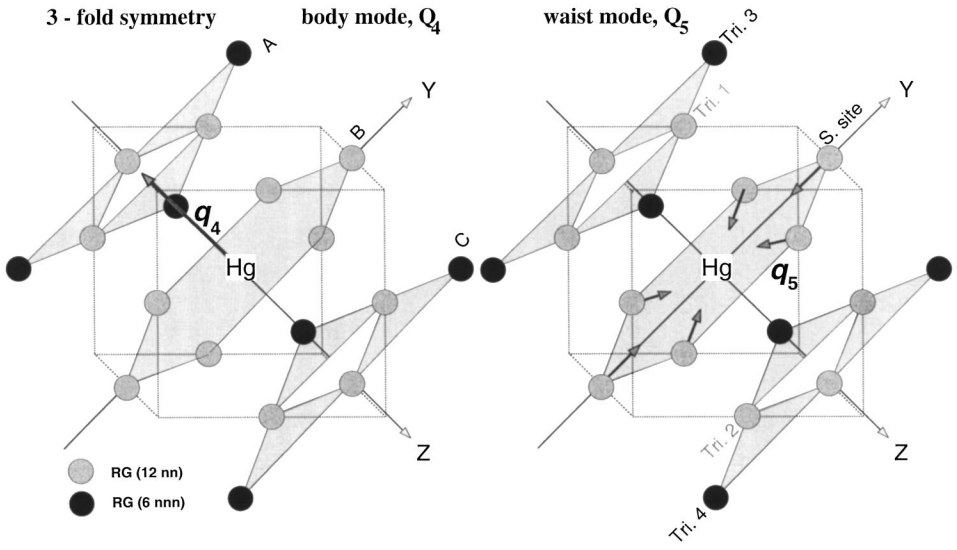

FIG. 4. The alternative guest atom-based coordinate system used to calculate the six-atom vibronic modes occurring for substitutional site occupancy. In it, the Z axis is chosen coincident with one of the four threefold symmetry axes of the cubo-octahedral fcc unit cell instead of the fourfold symmetry axes system shown in Fig. 1 for the four-atom modes. The X and Y axes are then located on the central hexagonal plane. The atoms located on the close packed A, B, and C planes are shown on the shaded background. In the six-atom body mode (Q_4), depicted on the left-hand side, the metal p_z-orbital atom moves along the Z axis perpendicular to the close-packed planes. For the six-atom waist mode (Q_5), shown on the right-hand side, the 6 NN atoms move in phase on plane B, towards the guest metal atom.

mode of Hg/Xe are presented in the lower half of Fig. 3. As shown by the solid curves in the lower right panel of this figure, this mode leads to excited state stabilization only for the p_z orbital orientation. These body and waist mode calculations are consistent with the behavior seen in earlier four-atom calculations[5] on the $Zn(^1P_1)/RG$ systems.

2. Trigonal (six-atom) symmetry modes

Calculation of the six-atom modes involves a 45° rotation of all three axes used for the four-atom modes, such that the Z axis is coincident with one of the four, threefold symmetry axes of the $Hg \cdot RG_{12}$ cubo-octahedron. As shown in Fig. 4, this coordinate system results in a perpendicular intersection of the Z axis through the centers of the two end triangles and the central hexagon of rare gas atoms with the X and Y axes in the plane of the regular hexagon. In this arrangement, the 12 nearest neighbor atoms surrounding the metal atom are positioned as 3, 6, and 3 atoms on planes perpendicular to the Z axis. The associated two triangles and hexagon are located on the close-packed A, B, and C planes of the fcc structure.

To achieve the required p-orbital degeneracy in the substitutional site, the six next nearest neighbor atoms in the second sphere surrounding the guest metal atom must be included. The six additional atoms are arranged, as shown in Fig. 4, in the larger triangles on the A and C planes at a distance of the lattice parameter, a, from the guest metal atom. Two types of six-atom modes are identified in the excited state. One involves the in-phase contraction of the six rare gas atoms on the X/Y plane towards the central metal atom. The other is motion of the metal atom along the Z axis.

a. The six-atom body mode: Q_4, as illustrated on the left-hand side of Fig. 4, involves perpendicular motion of the excited state Hg atom from the center of the hexagon of rare gas atoms on plane B to either plane A or C. The geometric details of the five categories of $Hg \cdot RG$ interactions[5] identified for the Q_4 mode are presented in Appendix A. The potential energy curves obtained by summing the five interactions, are shown by the solid traces in the top of Fig. 5 for the Hg/Xe system. In contrast to the four-atom body mode,

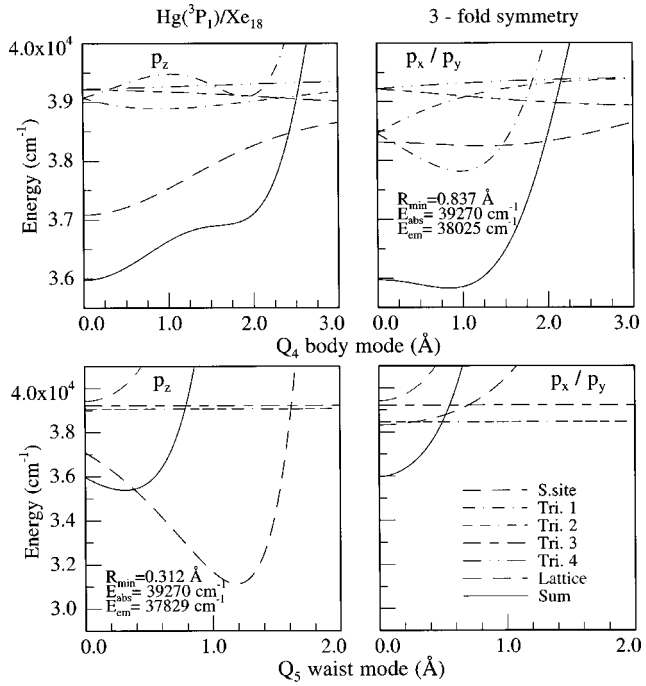

FIG. 5. Energetics calculated for the five specific interactions involved in the six-atom body (Q_4) and waist (Q_5) mode for the Hg/Xe system are shown by the legend used. The total potential energy curves obtained by summing these five interactions and the lattice contribution are shown by the solid line.

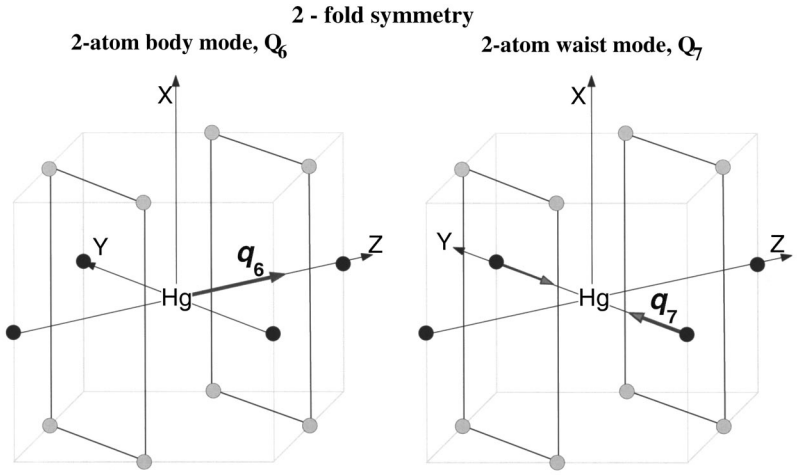

FIG. 6. A representation of the coordinate system used for the two-atom body and waist modes Q_6 and Q_7, respectively, calculations. The coordinate system has been chosen to coincide with the one of the twofold symmetry axes of the cubo-octahedron.

the $^3A_1(p_z)$ state in the six-atom body mode is not stabilized. The lack of stabilization evident in Fig. 5, arises from strong destabilization occurring with movement of the metal (p_z) orbital away from the hexagon (S site) on plane B and the initially repulsive interaction it experiences as it approaches the 3 NN Xe atoms positioned as a triangle on planes A or C. The latter repulsive interaction is shown by the dashed–dotted line (Tri 1) in Fig. 5, the former destabilization by the dashed line (S site). However, the ^3E state of this mode, corresponding to the degenerate p_x/p_y orbital orientations of the excited $^3P_1$ Hg atom, is slightly stabilized. The stabilization arises from the approach of the Hg p_x/p_y orbital to the three NN atoms arranged as a triangle (Tri 1) on plane A. This is nearly counteracted by the destabilization incurred by movement away from the other NN triangle (Tri 2) on plane C, resulting in only a small net stabilization.

b. The six-atom waist mode: Q_5 involves, as shown on the right in Fig. 4, in-phase contraction of six NN lattice atoms on the close-packed B plane towards the central metal atom. The total energies of the excited $^3A_1(p_z)$ and $^3E(p_x/p_y)$ states in the waist mode of the $\mathrm{Hg}(^3P_1)\cdot\mathrm{RG}_{18}$ cluster obtained from Eqs. (2)–(4) are given by the expressions

$$\begin{aligned}\mathbf{W}_{^3\mathbf{A1}}(\mathbf{R}) = {} & 6[\cos^2\theta_A V_{^3\Sigma}(R_1) + \sin^2\theta_A V_{^3\Pi}(R_1)] \\ & + 6[\cos^2\theta_B V_{^3\Sigma}(R_1) + \sin^2\theta_B V_{^3\Pi}(R_1)] \\ & + 6[\cos^2\theta_C V_{^3\Sigma}(R_2) + \sin^2\theta_C V_{^3\Pi}(R_2)] \\ & + \sum_{i=1}^{m} V^X_{\mathrm{Rg-Rg}}(r_i), \end{aligned} \tag{8}$$

$$\begin{aligned}\mathbf{W}_{^3\mathbf{E}}(\mathbf{R}) = {} & 3[\sin^2\theta_A V_{^3\Sigma}(R_1) + [\cos^2\theta_A + 1] V_{^3\Pi}(R_1)] \\ & + 3[\sin^2\theta_A V_{^3\Sigma}(R_1) + [\cos^2\theta_A + 1] V_{^3\Pi}(R_1)] \\ & + 3[\sin^2\theta_A V_{^3\Sigma}(R_2) + [\cos^2\theta_A V_A + 1] V_{^3\Pi}(R_2)] \\ & + \sum_{i=1}^{m} V^X_{\mathrm{Rg-Rg}}(r_i), \end{aligned} \tag{9}$$

in which the angles θ_A, θ_B, and θ_C are defined with respect to the Z axis and have values of $\pi/5.104\,299$, $\pi/2$ and $\pi/3.288\,535$ radians. R_1 and R_2 refer to the nearest neighbor $(a/\sqrt{2})$ and next nearest neighbor (a) distances, respectively.

In the calculation of the energetics of the six-atom waist mode, only the distance of the six Hg–RG interactions on plane B (R_1) is decreased, as shown on the right-hand side of Fig. 4. Although the cluster size is restricted to an $\mathrm{M}\cdot\mathrm{RG}_{18}$ species, 24 additional on-plane RG–RG interactions arising inside the fourth surrounding sphere, are included. This term $[m=24$ in Eq. (8)] is required[16] to account for the strong lattice destabilization that occurs on the close packed plane B from contraction of the equilibrium rare gas distances. The results of the six-atom waist mode calculations are shown on the bottom of Fig. 5 for the Hg/Xe system. As indicated by the dashed lines in this figure, stabilization arises only for the p_z orbital orientation with the contraction of the six Hg–RG bonds on plane B. Strong destabilization, shown by the broken gray line, comes from disruption of the NN Rg–Rg distances on the close packed B plane of the lattice, greatly reducing the overall stabilization (solid trace) of this mode.

3. Twofold (two-atom) symmetry modes

Calculation of the two-atom modes involves a 45° rotation of the Z and Y axes about the X axis from the coordinate system used[5] for the four-atom modes, where the Cartesian axes were coincident with the three, fourfold symmetry axes. Figure 6 shows the resulting arrangement of the 12 nearest neighbor RG atoms around the guest metal atom in the substitutional site. When counted along the Z axis, there is a 1, 4, 2, 4, 1 arrangement of the 12 NN RG atoms on this axis with the metal atom at the origin. It can be seen in Fig. 6 that there are two NN on both the Z and Y axes with the remaining eight NN atoms located in two rectangles at right angles to the Z axis. Two types of two-atom modes are identified in the excited state. One involves the in-phase contraction of the two NN rare gas atoms on the Y axis towards the central metal atom. The other is motion of the metal atom along the Z axis directly towards one NN atom.

a. Two-atom body mode, Q_6: This mode involves motion of the excited state metal atom on the Z axis towards one of the 12 NN RG atoms positioned on this axis. It is

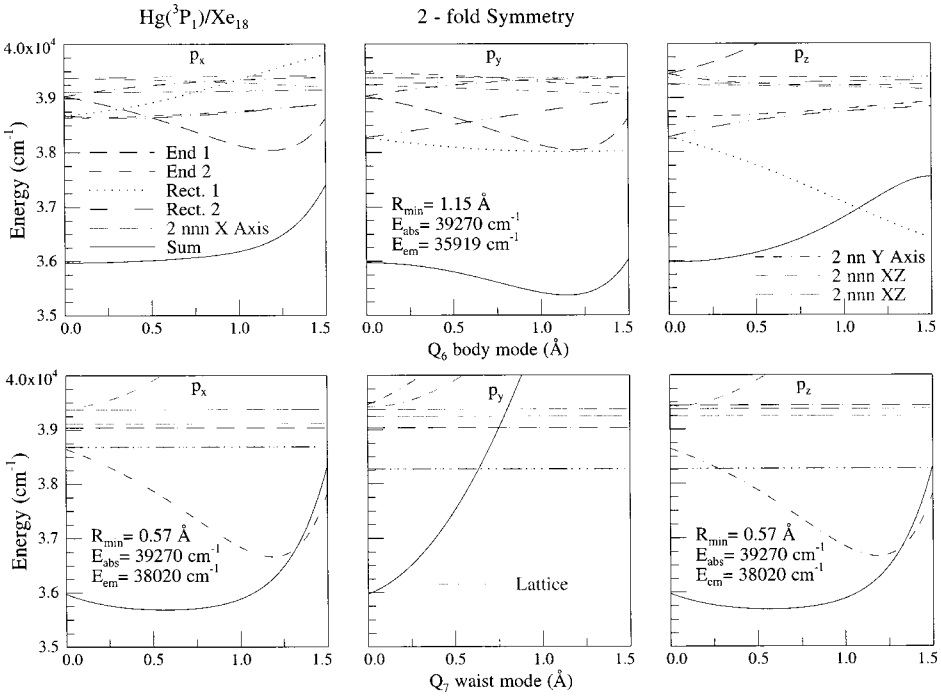

FIG. 7. Energetics calculated for the eight specific interactions involved in the two-atom body (Q_6) and waist (Q_7) modes depicted in Fig. 6. The potential energy curves obtained by summing these eight interactions for the three p-orbital orientations are shown by the solid lines for Hg/Xe.

illustrated on the left-hand side in Fig. 6 and involves passage of the excited state metal atom through the 4 NN RG atoms arranged as a rectangle perpendicular to the Z axis. With the length of the sides of this rectangle, the lattice parameter (a) and substitutional site size (SS), the distance of each of the four rare gas atoms to the center of the rectangle is then $R_{\text{c.m.}}=(3/8)^{1/2}a$. Using the associated values of ϕ_k in Eqs. (3) and (4), $\phi_1=(\frac{1}{2})\cos^{-1}(\frac{1}{3})$, $\phi_2=\pi-[(\frac{1}{2})\cos^{-1}(-\frac{1}{3})]$, $\phi_3=[(\frac{1}{2})\cos^{-1}(\frac{1}{3})]+\pi$, and $\phi_4=2\pi-[(\frac{1}{2})\cos^{-1}(\frac{1}{3})]$ the following expressions were obtained for the $^3B_1(p_x)$ and $^3B_2(p_y)$ states:

$$p_y \Rightarrow W_{B2}(R)=\tfrac{4}{3}[V_\Sigma(R)\sin^2\theta_k+V_\Pi(R)(\cos^2\theta_k+2)], \tag{10}$$

$$p_x \Rightarrow W_{B1}(R)=\tfrac{8}{3}[V_\Sigma(R)\sin^2\theta_k+V_\Pi(R)(\cos^2\theta_k+\tfrac{1}{2})]. \tag{11}$$

The following expression for the $^3A_1(p_z)$ electronic state was obtained from Eq. (2):

$$p_z \Rightarrow W_{A1}(R)=4[V_\Sigma(R)\cos^2\theta_k+V_\Pi(R)\sin^2\theta_k]. \tag{12}$$

Details of the eight specific interactions [labeled (i)–(viii)] involved in this mode are presented in Appendix B. The potential energy curves calculated for the interactions (i)–(viii) involved in the two-atom body mode, Q_6 are shown for the Hg/Xe system in Fig. 7. The potential energy curves for Q_6 are obtained by the summation of the eight interactions, and are shown by the solid traces in Fig. 7. Only the p_y orbital orientation leads to stabilization[17] for the Q_6 mode in Hg/Xe.

b. Two-atom waist mode, Q_7: The two-atom waist mode calculation involves, as shown on the right-hand side of Fig. 6, the in-phase contraction of two nearest neighbor rare gas atoms on the Y axis to the central metal atom. The overall energies of the excited $^3A_1(p_z)$, $^3B_1(p_x)$, and $^3B_2(p_y)$ $^3P_1$ states of the mercury atom in the $M\cdot RG_{18}$ cluster are obtained from Eqs. (2), (3), and (4). For the $^3A_1(p_z)$ state the following expression is used:

$$\begin{aligned}\mathbf{W}_{^3\mathbf{A1}}(\mathbf{R})=&\,2[\cos^2\theta_A V_{^3\Sigma}(R_1)+\sin^2\theta_A V_{^3\Pi}(R_1)]\\&+8[\cos^2\theta_B V_{^3\Sigma}(R_1)+\sin^2\theta_B V_{^3\Pi}(R_1)]\\&+2[\cos^2\theta_C V_{^3\Sigma}(R_1)+\sin^2\theta_C V_{^3\Pi}(R_1)]\\&+4[\cos^2\theta_D V_{^3\Sigma}(R_2)+\sin^2\theta_D V_{^3\Pi}(R_2)]\\&+2[\cos^2\theta_E V_{^3\Sigma}(R_2)+\sin^2\theta_E V_{^3\Pi}(R_2)]\\&+\sum_{i=1}^{m} V^X_{\text{Rg-Rg}}(r_i).\end{aligned} \tag{13}$$

In this equation the angles θ_A, θ_B, θ_C, θ_D, and θ_E are defined with respect to the Z axis and have values of 0, $\pi/3$, $\pi/2$, $2\pi/3$, and π radians, respectively. R_1 and R_2 refer to the nearest neighbor distance and the next nearest neighbor distances, respectively.

Results calculated for the Q_7 mode are shown on the bottom in Fig. 7 for Hg/Xe. Excited state stabilization occurs for both the p_x and p_z orbital orientations, whereas p_y is strongly repulsive due to the pure Σ interaction with the two approaching rare gas atoms on the Y axis. The p_x and p_z orbitals, although arising from different electronic states of the excited state Hg $^3P_1$ atom, show the same excited state minimum due to symmetry.

Lattice destabilization must also be included in these calculations as the waist mode Q_7 involves motion of two rare gas atoms with respect to their nearest neighbors. Since the RG atoms initially occupying equilibrium positions in the lattice, any displacement from these positions will destabilize the host lattice. 22 RG–RG interactions were considered, of which the motion of the two RG atoms on the Y-axis

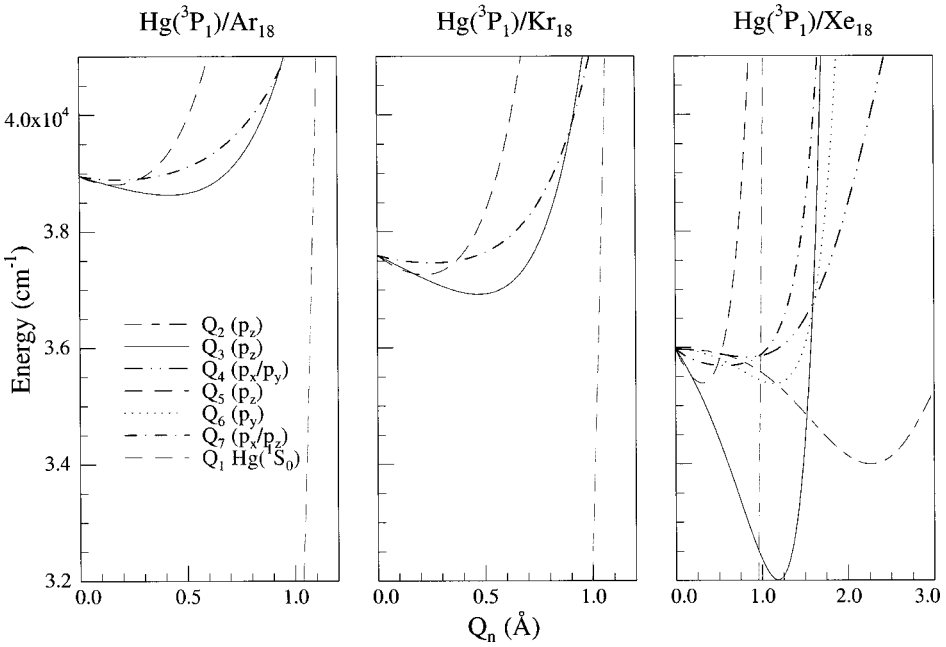

FIG. 8. A comparison of the excited $Hg(^3P_1)$ state potential energy curves of the vibronic modes exhibiting stabilization in the Hg/RG systems. Shown also is the ground $Hg(^1S_0)$ state potential energy curves calculated for the breathing mode, Q_1. Particularly noteworthy is the crossing of this curve with the very strongly stabilized four-atom modes in the Hg/Xe system.

towards a rectangle of its nearest neighbors is the most important. This repulsive lattice interaction is represented by the gray line in the bottom panels in Fig. 7, and reduces considerably the stabilization of these modes for the p_x and p_z orbital orientations.

III. DISCUSSION

A summary of the excited state calculations conducted on the three Hg/RG systems is presented in Fig. 8. In making this plot, identical calculations to those shown in detail for the Hg/Xe system were performed on the Hg/Ar and Hg/Kr systems. However, only the modes exhibiting stabilization are shown, as they are the only ones that will lead to Stokes-shifted emission.

As indicated by the solid curves in Fig. 8, the four-atom waist mode, Q_3, leads to excited state stabilization for all the Hg/RG systems but only for the p_z orbital orientation. In contrast, the four-atom body mode, Q_2, exhibits stabilization only in the Hg/Xe system. The $^3A_1(p_z)$ state in the six-atom body mode, Q_4, is not stabilized in any of the solid rare gases. It is evident in the detailed Hg/Xe plot shown in Fig. 5, that the reason for the lack of stabilization is the repulsive interaction the metal (p_z) orbital experiences as it approaches the three NN Xe atoms positioned as a triangle on planes A or C. This repulsive interaction (shown for Hg/Xe in Fig. 5 by the dot-dashed line, Tri 1), is much stronger in Hg/Kr and stronger still in Hg/Ar as the lattice parameters get smaller. The $^3E(p_x,p_y)$ state of this mode shows a shallow minimum in Hg/Xe. The six-atom waist mode, Q_5, exhibits excited state minima in the p_z orbital orientation for all the Hg/RG systems.

Stabilization is not found for the two-atom body mode, Q_6, in any of the orbital orientation for Hg isolated in Ar and Kr. However, the p_y orbital orientation exhibits a stabilization for the body mode, Q_6, in Hg/Xe. In contrast, the waist mode of this symmetry, Q_7, is stabilized for the p_x,p_y orbital orientations in all three rare gas systems. In the next section a comparison of the predicted absorption and emission is made with recorded matrix data.

A. Absorption energies

The absorption energy of the guest mercury atom isolated in a solid rare gas lattice is calculated as the difference between the ground $Hg(^1S_0)\cdot RG_{18}$ and the excited state $Hg(^3P_1)\cdot RG_{18}$ cluster energies. Within the Frank–Condon approximation no movement will occur between the Hg and the cluster atoms during the electronic transition, so the absorption energy is given by

$$E_{\mathrm{abs}} = E[\mathrm{Hg}(^3P_1)\cdot \mathrm{RG}_{18}]_{Q(R=0)} - E[\mathrm{Hg}(^1S_0)\cdot \mathrm{RG}_{18}]_{Q(R=0)}, \quad (14)$$

where $Q(R=0)$ represents zero displacement for a vibronic mode, Q_n (corresponding to the center of a substitutional site). Accordingly, for a given site occupancy, the calculated absorption energies must be identical for all vibronic modes. The level of agreement between the four-atom modes and the new six-atom and two-atom mode calculations is evident for Hg/Xe in Figs. 3, 5, and 7 by the identical E_{abs} values $(39\,270\ \mathrm{cm}^{-1})$ obtained for the Q_3, Q_4, and Q_5 modes.

TABLE II. A comparison of the observed absorption wavelengths (nm units) for the $^3P_1 \leftarrow {}^1S_0$ transition of matrix-isolated atomic mercury with the calculated absorption values. The difference between the observed band maxima and the predicted values are quoted as $\delta_{\mathrm{obs-calc}}$ in cm^{-1}. For a given Hg/RG system, the quoted predicted value was found for the three symmetry systems used, the three p-orbital orientations and the body and waist vibronic modes.

Hg/RG	E_{calc}	λ_{calc}	λ_{obs}	$\delta_{\mathrm{obs-calc}}$
Hg/Ar	40 495	246.94	246.0	+155
Hg/Kr	39 922	250.49	249.1	+227
Hg/Xe	39 270	254.65	253.4	+192

Table II shows a comparison of the observed absorption wavelengths with those calculated for substitutional site occupancy.

The 246.94 nm absorption wavelength calculated for Hg/Ar, compares very well with the observed[2] band center at 246 nm. The recorded[2] absorption band center for Hg isolated in solid Kr is at 249.1 nm while the calculated value is 250.49 nm. Better agreement with observed data is achieved in Hg/Xe where the calculated value of 254.64 nm compares favorably with the observed[2] absorption centered at 253.4 nm. From the comparison presented in Table II, it is clear that the calculated absorptions match the red component of the threefold-split bands for all three Hg/Rg systems. It thereby supports the assumption of substitutional site occupancy inherent in the pair-potential calculations conducted. It is not within the scope of the present calculations to examine the threefold absorption splitting effect because as indicated by Eq. (14), the absorption values are determined at the center of the substitutional site, i.e., at $R=0$ only. Simulation[18] of the Jahn–Teller structure on the absorption profiles requires displacement of the ground state metal atom from the center of the substitutional site, a task difficult to implement in the code developed for the calculations presented in the present theoretical paper.

B. Emission energies

The $\mathrm{Hg}(^3P_1 \rightarrow {}^1S_0)$ emission energies are calculated with the formula

$$E_{\mathrm{em}} = E[\mathrm{Hg}(^3P_1)\cdot \mathrm{RG}_{18}]_{Q(R_{\mathrm{min}'})} - E[\mathrm{Hg}(^1S_0)\cdot \mathrm{RG}_{18}]_{Q(R_{\mathrm{min}'})}, \quad (15)$$

where $R_{\mathrm{min}'}$ represents the nuclear configuration of a given excited state vibronic mode, Q, at its energy minimum. In accordance with the Franck–Condon approximation, the energy of this vibronic mode on the ground state is obtained at the $R_{\mathrm{min}'}$ value identified in the excited state. The results calculated in this way for the vibronic modes exhibiting excited state stabilization (shown in Fig. 8) in the Hg/RG systems are collected in Table III.

Hg/Ar: The four-atom (p_z), six-atom (p_z) and two-atom (p_x and p_z) waist modes exhibit excited state stabilization in solid argon. The emission wavelengths calculated for these Q_3, Q_5, and Q_7 modes are 256.14, 250.51, and 248.29 nm, respectively. From the comparison made in Fig. 8 of the three excited state vibronic modes, it is expected that Hg/Ar emission is dominated by the six-atom waist mode, (Q_5) as it exhibits more rapid stabilization (i.e., a steeper gradient) than the more deeply bound four-atom waist, (Q_3) or the two-atom waist mode. As shown in Fig. 9, the 250.51 nm emission calculated for the Q_5 mode closely matches the deconvoluted central component at 250.69 nm in the observed[2] band. The two other predicted emission bands lie to the blue and red of the two remaining deconvoluted emission components.

Hg/Kr: As found in Hg/Ar, only the $Q_3(p_z)$, $Q_5(p_z)$, and $Q_7(p_x,p_y)$ modes exhibit excited state stabilization in Hg/Kr leading to predicted emission at 261.16, 256.12, and 252.71 nm, respectively. The six-atom waist mode Q_5 in this system also exhibits the steepest stabilization gradient (middle plot of Fig. 8) and is therefore expected to dominate the emission. The associated predicted emission at 256.12 nm is red of the deconvoluted central component at 254.22 nm. The two-atom waist mode at 252.7 nm agrees well with the blue component at 253.25 nm. As in the Hg/Ar system, the four-atom waist mode (261 nm) is red of the deconvoluted red component (255 nm).

Hg/Xe: Stabilization was found in Hg/Xe for the six excited state vibronic modes shown on the right-hand side of in Fig. 8. In addition to the three modes stabilized in the Hg/Ar and Hg/Kr systems, the Q_2 (fourfold symmetry, p_z), Q_4 (threefold symmetry p_x, p_y) and the Q_6 (twofold symmetry p_y) modes are stabilized in Hg/Xe. The calculated emission

TABLE III. A comparison of the calculated Hg atom $^3P_1 \rightarrow {}^1S_0$ emission wavelengths with the experimental data reported in Refs. 2 and 3 for the Hg/Ar, Hg/Kr, and Hg/Xe systems. All the vibronic modes of $\mathrm{Hg}\cdot\mathrm{RG}_{18}$ clusters which lead to excited state stabilization are presented and compared with the bands deconvoluted in Gaussian fits of the emission bands centered at 250.3, 254.1, and 273 nm in Ar, Kr, and Xe, respectively.

Hg/RG	Mode	Motion	Calculated $E(\mathrm{cm}^{-1})/\lambda(\mathrm{nm})$	Observed $E(\mathrm{cm}^{-1})/\lambda(\mathrm{nm})$
Hg/Ar	Q_3 (p_z)	4-waist	39 041/256.14	39 719/251.77
	Q_5 (p_z)	6-waist	39 919/250.51	39 890/250.69
	Q_7 (p_x, p_z)	2-waist	40 275/248.29	40 034/249.78
Hg/Kr	Q_3 (p_z)	4-waist	38 290/261.16	39 149/255.43
	Q_5 (p_z)	6-waist	39 044/256.12	39 335/254.22
	Q_7 (p_x, p_z)	2-waist	39 571/252.71	39 487/253.25
Hg/Xe	Q_2 (p_z)	4-body	27 875/358.74	N/A
	Q_3 (p_z)	4-waist	26 474/377.73	N/A
	Q_4 (p_x, p_y)	6-body	38 025/262.98	
	Q_5 (p_z)	6-waist	37 829/264.34	36 619/273.08
	Q_6 (p_y)	2-body	35 919/278.40	35 729/279.88
	Q_7 (p_x, p_z)	2-waist	38 020/263.02	37 535/266.42

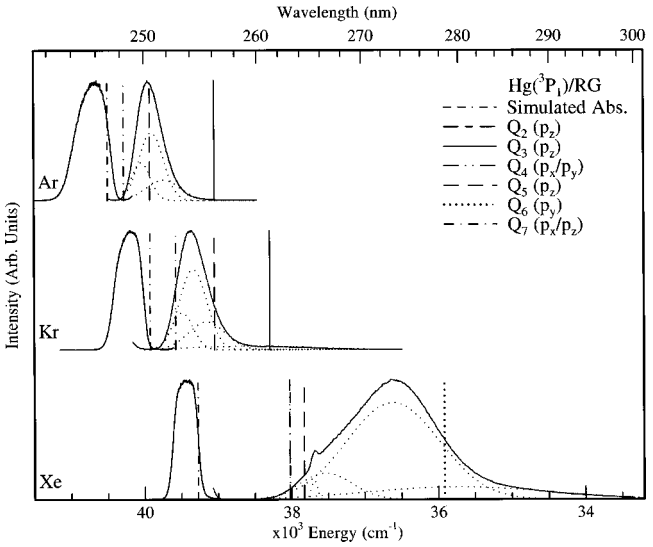

FIG. 9. A comparison of the observed and calculated atomic Hg ($^3P_1 \leftrightarrow {}^1S_0$) spectroscopy. The experimental spectra shown were recorded at 12 K and the underlying dotted lines show the deconvoluted components extracted in the Gaussian line shape fits shown in the preceding paper (Ref. 3).

wavelengths are, as collected in Table III, at 358.74, 377.73, 262.98, 264.34, 278.4, and 263.02 nm for the $Q_2(p_z)$, $Q_3(p_z)$, $Q_4(p_x/p_y)$, $Q_5(p_z)$, $Q_6(p_y)$, and $Q_7(p_x,p_z)$ modes, respectively. The predicted $Q_6(p_y)$ value at 278.4 nm provides the best match with the red emission component at 279.88 nm. Stabilization of this mode, the two-atom body mode, is due to the favorable interaction between the Hg atom p_y orbital and a single Xe atom. This attractive interaction with one Xe atom is possible only for the $\Pi(p_y)$ orbital as the metal atom in this orientation can pass through the long side of the rectangle of NN Xe atoms, whose length is the lattice parameter, a, without experiencing strong repulsive interactions. In contrast, motion in the $\Pi(p_x)$ orbital orientation involves, as shown on the left-hand side Fig. 6, passage through the short side of the rectangle which, a substitutional site size in length, and experiences repulsive interaction as indicated by the dotted lines in Fig. 7. The six-atom waist mode yields emission at 264.34 nm to the blue of the deconvoluted blue component at 273.08 nm. The remaining two modes in Hg/Xe (Q_4 and Q_7) are located at 263 nm in the vicinity of the blue deconvoluted component at 266 nm.

Conspicuous in Fig. 8 is the fact that the four-atom body Q_2 and waist Q_3 modes of Hg/Xe exhibit much larger excited state stabilization energies than the two- and six-atom modes. Thus, an obvious question arises as to the role these modes play in emission as it is very likely that the former modes will lead to some relaxation of the excited state population. This is especially so for the 377 nm, four-atom waist mode, Q_3, as it exhibits a steep stabilization gradient, so that even at low temperatures, excited state relaxation must occur along this vibronic mode. At higher temperatures, the branching ratios should favor the strongly stabilized modes leading to a reversible enhancement of the Q_2 and Q_3 modes (358 and 377 nm, near-UV bands) at the expense of the six-atom waist mode Q_5 (273 nm, UV band) and the two-atom body mode.

According to the present Hg/Xe_{18} calculations, the Q_2 and Q_3 modes are predicted to produce emission in the near-UV (350–400 nm) spectral region where mercury dimer and several unassigned emission bands have recently[19] been observed in Hg/Xe samples. Hg/Xe samples prepared by our group showed no atomic emission in the near-UV and no reversible temperature dependence was observed. However, the growth of Hg_2 bands was observed with prolonged atomic excitation, signaling that nonradiative processes must be considered which quench the atomic emission. The following quenching mechanism has become evident in our pair-potentials calculations of Hg/Xe and is illustrated in Fig. 8.

It involves the deeply bound, four-atom excited state vibronic modes being crossed by the breathing mode of the electronic ground state. The breathing mode, Q_1, involves in-phase motion of the 12 nearest neighbor atoms and the curves calculated with Eq. (1) for the Hg/Ar, Hg/Kr, and Hg/Xe systems are shown in Fig. 8. It is clear in this figure that Hg/Xe is the only system exhibiting a crossing between stabilized excited state vibronic modes and the repulsive ground state. The origin of this difference lies in the much greater stabilization the Hg/Xe four-atom modes exhibit compared with the corresponding modes in the Hg/Ar and Hg/Kr systems. Quenching will then arise for the most strongly stabilized excited state modes in Hg/Xe due to their crossing with the ground state. Because of the large spin–orbit coupling in atomic mercury, the crossing of these states of different spin will give rise to very efficient intersystem crossing and will quench the near-UV emission.

Although emission quantum yields have not been measured in the Hg/RG systems it is known that prolonged excitation of the atomic resonance in Hg/Xe produces mercury dimer. Thus the quenching mechanism presented would also rationalize this surprising observation of photoclustering in a solid which ideally accommodates atomic mercury. Thus the atomic quenching mechanism will dispose up to 30 000 cm^{-1} energy into the host lattice, providing sufficient energy for the migration of the atomic mercury in the solid.

IV. CONCLUSIONS

From the close agreement found with observed absorption energies,[2] pair-potentials calculations indicate that atomic mercury occupies essentially undistorted substitutional sites in solid Ar, Kr, and Xe. Calculation of the excited state energies for Hg/Ar and Hg/Kr show that three vibronic modes lead to emission in these matrices. Of these, the six-atom waist mode, Q_5, is expected to dominate the low temperature spectra as it has the steeper stabilization gradient. In Hg/Ar matrices, this mode predicts emission in close agreement with the observed bands but in Hg/Kr it is slightly to the red of the observed band.[2] Hg/Xe calculations indicate that emission can arise from six modes. The two-atom body $Q_6(p_y)$ mode leads to emission which most closely matches the observed[19] band center at 273 nm. This mode involves motion of the $Hg(p_y)$ atom to one of the 12 NN Xe atoms and corresponds to the proposal made by Crepin and Tramer, that excimer type behavior was responsible for the emission in Hg/Xe. However, the results presented here indicate that this motion must occur in a specific orbital orientation (p_y) to achieve stabilization and so produce emission.

Calculations conducted on the four-atom waist (Q_3) and the four-atom body modes (Q_2) predict wavelength emission in the 350–400 nm region in Hg/Xe which has never been detected in the spectra recorded. A quenching mechanism of these modes is identified in the calculations, involving the crossing of these strongly bound, excited state vibronic states by the repulsive ground state potential. This crossing does not occur in the Hg/Ar and Hg/Kr systems.

ACKNOWLEDGMENTS

This research was funded by the Irish Government *Forbairt* SC/96/422 and *Enterprise Ireland*, SC/98/403 Basic Science research grants the latter to whom M.C. gratefully acknowledges receipt of a Ph.D. studentship.

APPENDIX A: GEOMETRIC DETAILS OF THE FIVE SPECIFIC INTERACTION IN THE THREEFOLD SYMMETRY MODES

Five categories of the Hg·RG interactions are identified in the calculation of the threefold symmetry, six-atom modes of the $Hg \cdot RG_{18}$ clusters. The geometric details are illustrated in Fig. 4.

(i) S site/$W(R_1,\theta_1)$, motion of the Hg atom away from the hexagon of six NN atoms on plane B.

(ii) Tri $1/W(R_2,\theta_2)$, motion towards the center of the three NN atoms on plane A (small, light shaded triangle). The separation between the close packed A, B, and C planes, b, is $\sqrt{(2/3)}$SS.

(iii) Tri $2/W(R_3,\theta_3)$, motion away from the three NN atoms on plane C (small, light triangle), i.e., the opposite of (ii).

(iv) Tri $3/W(R_4,\theta_4)$, motion towards the three NNN atoms indicated by the large, dark shaded triangle on plane A. These atoms are initially at a lattice parameter distance, a, from the guest metal atom in the substitutional site.

(v) Tri $4/W(R_5,\theta_5)$, motion away from three NNN atoms on plane C, the opposite of (iv).

The same interactions are included in calculation of the six-atom waist mode. However, this mode involves only a single variable, R_1, *viz*, the Hg atom nearest neighbor distance on plane B.

APPENDIX B: GEOMETRIC DETAILS OF THE EIGHT SPECIFIC INTERATIONS IN THE TWOFOLD SYMMETRY MODES

Calculation of the two-atom modes for a Hg/RG_{18} cluster involves consideration of the eight interactions illustrated in Fig. 6. They are as follows:

(i) End $1/W(R_1,\theta_1)$, motion of the Hg atom from the substitutional site towards one of the nearest neighbor atoms on the Z axis. $R_1 = \mathrm{SS} - x$ where x represents displacement along the Z axis.

(ii) End $2/W(R_2,\theta_2)$, the motion of the metal atom away from the other NN on the Z axis. This is the opposite of interaction (i) and the distance is $R_2 = \mathrm{SS} + x$.

(iii) Rect $1/W(R_3,\theta_3)$, this interaction involves approach to the rectangle of four NN atoms. Initially the $Hg(p_z)$ atom is at a distance SS/2 from the center of mass of the rectangle. During the motion this distance becomes $\mathrm{SS}/2 - x$. The distance from each of the RG atoms to the center of mass of the rectangle is $r = (3/8)^{1/2}a$, so this interaction occurs at a distance $R_3 = [(\mathrm{SS}/2 - x)^2 + ((3/8)^{1/2}a)^2]^{1/2}$ and the angle $\theta_3 = a \sin(r/R_3)$.

(iv) Rect $2/W(R_4,\theta_4)$, this interaction is the motion of the excited state guest atom away from the rectangle of four NN. It is the opposite of interaction (iii), therefore $R_4 = [(\mathrm{SS}/2 + x)^2 + ((3/8)^{1/2}a)^2]^{1/2}$ and $\theta_4 = a \sin(r/R_4)$.

(v) Two NN $Y/W(R_5,\theta_5)$, motion of the metal atom away from the two NN rare gas atoms on the Y axis. This interaction takes place at $R_5 = [(\mathrm{SS})^2 + (x)^2]^{1/2}$ where $\theta_5 = a \sin(\mathrm{SS}/R_5)$.

(vi) Two NNN $X/W(R_6,\theta_6)$ involves the interaction between the metal atom and the two NNN on the X axis. Initially these two rare gas atoms are at the next nearest neighbor distance of the lattice parameter a from the metal atom. During the motion the distance becomes $R_6 = [(a)^2 + (x)^2]^{1/2}$ where $\theta_6 = a \sin(a/R_6)$.

(vii) Two NNN $YZ/W(R_7,\theta_7)$, this motion involves approach of the Hg atom to the two NNN RG atoms positioned on the YZ plane on the diagonal initially at a distance a. $R_7 = [(\mathrm{SS} - x)^2 + (\mathrm{SS})^2]^{1/2}$ where $\theta_7 = a \sin(\mathrm{SS}/R_7)$.

(viii) Two NNN $YZ/W(R_8,\theta_8)$, this interaction is the opposite of (vii) and $R_8 = [(\mathrm{SS} + x)^2 + (\mathrm{SS})^2]^{(1/2)}$ and $\theta_8 = a \sin(\mathrm{SS}/R_8)$.

[1] M. McCarty and G. W. Robinson, Mol. Phys. **2**, 415 (1959).
[2] C. Crepin and A. Tramer, J. Chem. Phys. **97**, 4772 (1992).
[3] M. A. Collier and J. G. McCaffrey, J. Chem. Phys. **119**, 11878 (2003), preceding paper.
[4] W. H. Breckenridge, C. Jouvet, and B. Soep, in *Advances in Metal and Semiconductor Clusters*, edited by M. Duncan (JIA Press, Greenwich, CT, 1995), Vol. 3.
[5] J. G. McCaffrey and P. N. Kerins, J. Chem. Phys. **106**, 7885 (1997).
[6] J. Zuniga, A. Bastida, A. Requena, N. Halberstadt, and J. Beswick, J. Chem. Phys. **98**, 1007 (1993).
[7] S. Martrenchard-Barra, C. Jouvet, C. Lardeux-Dedonder, and D. Solgadi, J. Chem. Phys. **98**, 5281 (1993).
[8] M. H. Alexander, A. R. Walton, M. Yang, Y. Yang, E. Hwang, and P. J. Dagdigian, J. Chem. Phys. **106**, 6320 (1997).
[9] B. Healy and J. G. McCaffrey, J. Phys. Chem. A **104**, 3553 (2000).
[10] M. Okunishi, H. Nakazawa, K. Yamanouchi, and S. Tsuchiya, J. Chem. Phys. **93**, 7526 (1990).
[11] K. Fuke, S. Takayuki, and K. Kaya, J. Chem. Phys. **81**, 2591 (1984).
[12] S. L. Altmann and P. Herzig, *Point-Group Theory Tables* (Oxford Science, New York, 1994), p. 595.
[13] C. Kittel, *Introduction to Solid State Physics*, 5th ed. (Wiley, New York, 1976), p. 77.
[14] Preliminary lattice relaxation calculations reveal substitutional site expansions of only 0.067 and 0.015 Å for Ar and Kr, respectively, while a contraction of 0.026 Å is calculated for the Hg/Xe system. M. A. Collier and J. G. McCaffrey (unpublished).
[15] O. Roncero, J. Beswick, N. Halberstadt, and B. Soep, in *Dynamics of Poylatomic van der Waals Complexes*, edited by N. Halberstadt and K. Janda, NATO ASI Series Vol. 227 (Plenum, New York, 1990), p. 471.
[16] The Q_5 mode contrasts with the six-atom body mode, Q_4, for which the rare gas potential term does not appear since the latter involves only the motion of the guest metal atom and does not result in any changes in the positions of the lattice atoms.
[17] Note that the energy maximum present in the p_z body mode in the twofold symmetry is a result of the nonphysical behavior of the deconvoluted Hg·Xe Σ potential at short range.
[18] An alternative molecular dynamics approach which invokes a DIM method to probe vertical excitation energies of a very large number of ground state nuclear configurations is currently being applied to the mercury and other matrix-isolated metal atom systems. Initial results reveal the threefold absorption splitting assigned to the Jahn–Teller effect. P. dePujo, C. Crepin, and J. G. McCaffrey (unpublished).
[19] J. Helbing, A. Haydar, and M. Chergui, J. Chem. Phys. **113**, 3621 (2000).
[20] J. G. Kaup and W. H. Breckenridge, J. Phys. Chem. **99**, 13701 (1995).
[21] L. Laaksonen, J. Mol. Graphics **10**, 33 (1992).